Temperature dependence of NMR parameters calculated from path integral molecular dynamics simulations

Martin Dračínský,[a,*] *Petr Bouř,*[a] *Paul Hodgkinson*[b]

[a]Institute of Organic Chemistry and Biochemistry, Flemingovo nám. 2, 16610, Prague, Czech Republic

[b]Department of Chemistry, Durham University, South Road, DH1 3LE, Durham, UK

The influence of temperature on NMR chemical shifts and quadrupolar couplings in model molecular organic solids is explored using path integral molecular dynamics (PIMD) and density functional theory (DFT) calculations of shielding and electric field gradient (EFG) tensors. An approach based on convoluting calculated shielding or EFG tensor components with probability distributions of selected bond distances and valence angles obtained from DFT-PIMD simulations at several temperatures is used to calculate the temperature effects. The probability distributions obtained from the quantum PIMD simulations, which includes nuclear quantum effects, are significantly broader and less temperature dependent than those obtained with

conventional DFT molecular dynamics or with 1D scans through potential energy surface. Predicted NMR observables for the model systems were in excellent agreement with experiment.

Introduction

Solid-state nuclear magnetic resonance (SS-NMR) spectra provide valuable information about structure, interactions and dynamics in solids not available otherwise. In many aspects, SS-NMR spectroscopy is thus complementary to high-resolution x-ray diffraction methods. However, experimental NMR spectra cannot usually be related to the structure and dynamics of studied molecules in a straightforward manner. Ab initio computational methods must be used to predict NMR parameters, interpret the experimental data, and thus obtain information about system structure and dynamics.

It is well established that fast molecular motions, such as vibrations, conformational averaging, and molecular aggregation will change equilibrium values of NMR parameters.[1-12] Isotope shifts[13] and temperature dependence of NMR parameters are experimental manifestations of such dynamical averaging effects. Traditionally, quantum-chemical simulations of NMR parameters have been common for "isolated" molecules, such as those in gases or solutions. In the last decade, the gauge-including projector-augmented wave (GIPAW) procedure has been developed for routine predictions of magnetic resonance parameters in solids.[14] The power of the GIPAW approach for calculating NMR properties for fully periodic crystal structures, specifically in the context of organic solids, has been well documented in numerous studies.[1, 15-16] An alternative to the GIPAW approach are calculations of NMR parameters of molecular clusters, which allows application of a broader set of model chemistries, such as meta-GGA or DFT hybrid

functionals.[17-19] The quantum chemical calculations are typically performed using static structures, i.e. at 0 K and neglecting zero-point motion. However, dynamics can lead to significant discrepancies between computed and experimental data.

A straightforward way to handle the dynamical effects on molecular properties is a molecular dynamics (MD) simulation.[20-25] However, MD performed either with empirical or "first-principles" potentials treats nuclei as classical particles, and is not generally appropriate for molecules with discrete energy spectra. More precisely, when the energy of the excited states is larger than the Boltzmann thermal energy ($\Delta E >> k_B T$), application of MD is inappropriate because the system stays in the ground state.[26-27] At room temperature ($k_B T \sim 209$ cm^{-1} at 300 K), for example, this situation occurs for most high-frequency vibrational molecular motions, such as C–H stretching ($\Delta E \sim 3000$ cm^{-1}). On the other hand, averaging of the solvent positions and low-frequency molecular motions (e.g., semi-free rotation of covalent bonds) can be done with MD.

Nuclear quantum effects (NQE) including zero-point vibration, nuclear delocalisation and tunnelling are especially important for hydrogen atoms. These effects can be included through proper vibrational averaging,[17, 25-26] taking into account molecular flexibility, anharmonicities in nuclear potential, and realistic dependence of NMR parameters on the coordinates.[20, 28-29] Hydrogen bonds are particularly affected by dynamical and temperature effects, and both the potential energy landscape and chemical shift surfaces can be complex. Simplified approaches, such as the harmonic approximation, may fail to provide reliable vibrational corrections.[13, 30-31] Computations beyond the harmonic approximation are currently significantly limited due to their extensive demands on computer time and memory, and usually applied to individual molecules only. To obtain realistic results for larger systems, ad hoc approximations regarding the nuclear

potential or dependence of the spectral parameters on the geometry can be done.[32] For crystalline α-glycine only qualitative agreement with the experimental data was obtained with limited polynomial expansions of the potential and NMR properties around the equilibrium geometry. The temperature dependence of NMR shielding was significantly overestimated for most of the nuclei by this model.[33] For hydrogens, vibrational NMR corrections have been found to be transferable between similar molecules; no such transferability has been observed heavier nuclei, such as carbon, nitrogen, oxygen or fluorine.[34-35]

An alternative route to including quantum effects in quantum-chemical simulations is based on the wavefunction propagation using the Feynman's path integral[36] (PI) formalism. The path-integral MD (PIMD) methodology explored in the present study appears as a more universal way to account for the motional averaging. It accounts both for the temperature and quantum effects. The PI equations of motion are coupled with the usual MD procedures, in particular with those using DFT potentials for the nuclei and plane wave basis for the electronic wavefunction.

Recently, we introduced an approach for including NQEs in NMR calculations based on convoluting calculated shielding and coupling surfaces with probability distributions of relevant bond distances and valence angles obtained from PIMD simulations.[37] This approach systematically improved the agreement between calculated and experimental ^{13}C chemical shifts in solids. It also provided excellent predictions of deuterium isotope effects, which are easily detectable and can convincingly manifest the quantum nature of the nuclei. In particular, zero-point fluctuations lead to differences in vibrationally averaged NMR properties of natural and deuterated compounds. Similarly, the PIMD approach appeared suitable to describe hydrogen bonds stabilized by π-electron delocalization (resonance-assisted hydrogen bonds); when the

nuclear delocalisation was included in chemical shift calculations, the agreement with experiment was excellent, while static calculations showed very poor performance.

Here, we apply the PIMD approach to explain temperature dependence of solid-state NMR parameters of α-glycine and nitromalonamide. α-glycine is often used as secondary standard of carbon and nitrogen chemical shifts in solid-state NMR experiments, and it has been investigated in the temperature range 288-427 K using neutron diffraction;[38] no changes of molecular structure or phase transitions were observed under these conditions. The unit cell expands anisotropically with increasing temperature. The ^{13}C and ^{15}N chemical shifts of α-glycine over the temperature range 200–415 K was also reported.[39] For various polymorphic glycine forms, the plane wave pseudopotential methodology has been already successfully applied to produce static chemical shifts, although the static values sometimes significantly deviate from experiment.[40]

In the other studied system, solid 2-nitromalonamide (NMA, Figure 1), the O–H···O intramolecular hydrogen bond is one of the shortest hydrogen bonds known between oxygen atoms. The O···O distance obtained by X-ray diffraction at room temperature is 2.384 Å;[41] 2.391 Å was obtained at 15 K by neutron diffraction.[42] The enol hydrogen in the crystal is asymmetrically located between the two oxygen atoms, with distances of 1.14 Å for the O–H bond and 1.31 Å for the O···H contact. Previously, NQEs in solid NMA at 298 K have been studied by Car-Parrinello molecular dynamics with path integration. A very large delocalization of the O–H proton was found.[43]

The molecule is also interesting for a large anomalous temperature dependence of ^{2}H quadrupolar coupling in deuterated NMA. Normally, the magnitude of quadrupolar couplings is reduced with increasing temperature, due to vibrational and librational motions.[21] For NMA,

however, a 6.9 kHz increase was observed when temperature increased from 200 to 300 K.[44] Similar unusual temperature dependence of quadrupolar couplings has also been reported for other systems with short hydrogen bonds.[45-46] Previous ab initio calculations, even with high-level corrections for electron correlation, did not accurately reproduce such NMR data observed in such strongly hydrogen-bonded systems.[47-48] It has been shown that a simple model based on the anharmonicity of the hydrogen bond potential fails to describe temperature dependence of quadrupolar couplings.[24]

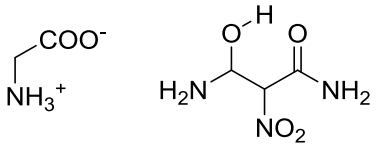

Figure 1. The structure of glycine and 2-nitromalonamide (NMA).

Methods

Structures of α-glycine determined by neutron diffraction at 200, 300 and 427 K (CSD refcodes GLYCIN91, GLYCIN20, GLYCIN24) and X-ray structure of nitromalonamide (refcode NMALAM) obtained from the Cambridge Crystallographic Database were used as initial geometries.[49] The unit cell of glycine contained four crystallographically equivalent molecules ($Z = 4$); $Z = 2$ for NMA. All calculations described in this work were performed for fully periodic systems (i.e. infinite crystals).

Born-Oppenheimer molecular dynamics (BOMD) simulations were run in the CASTEP program,[50] which is a DFT-based code, using an *NVT* ensemble, temperature of 200, 300 and 427 K, Langevin thermostat, 0.5 fs integration time step, ultrasoft pseudopotentials,[51] and planewave cutoff energy of 300 eV. Integrals were taken over the Brillouin zone using a Monkhorst-Pack[52] grid of the minimum k-point sampling of 0.1 $Å^{-1}$. Electron-correlation effects

were modeled using the generalized gradient approximation of Perdew, Burke, and Ernzerhof.[53] The atomic positions were optimized by energy minimization prior to the MD runs at the same computational level. The lattice parameters were fixed to the experimental values. No symmetry constraints were applied during the runs, as these are only relevant to the time-averaged structure. Simulations 10 ps long were performed for every compound. The path integral propagation was used on top of the BOMD simulations, with a Trotter decomposition of all nuclei into 16 beads. One PIMD simulation took ca two days on a computational cluster with 128 cores. It has been shown recently that calculated molecular properties of ice at 100 K using 16 beads in PIMD simulations were sufficiently close to those calculated with 32 beads. For example, dipole moments calculated with 16 and 32 beads differed less than 1%.[54] We have also performed the PIMD simulation at 50 K for GLYCIN97 structure, where the NQEs become more important. Here, 16 beads are insufficient, as shown by the unrealistically narrow distributions of distance probabilities observed in Figure S1. To further confirm that the Trotter decomposition into 16 replicas and the time step of 0.5 fs is sufficient for simulations of NQEs, we performed PIMD simulations at 200 and 300 K with 32 beads, and at 300 K with 16 beads and a shorter time step of 0.25 fs. The resulting distance probability distributions were almost identical to those obtained with 16 beads and 0.5 fs (shown in the SI). Discussion of the convergence of the NQEs with the number of beads is also discussed in Refs.[55-57]

To check reliability of the distance and angular probability distributions obtained under the periodic boundary conditions, MD simulation on a "supercell" of GLYCIN20 structure with the *c* dimension doubled was performed as well; resulting probability distributions were almost equal to those obtained with the smaller unit cell (see Figure S3 in the SI). To check convergence of the probability distributions with respect to the time of the simulations, we produced the angle

and distance probabilities for the second half of the GLYCIN20 PIMD simulation only (5–10 ps); these probability distributions were almost identical to those obtained from the whole simulation.

The temperature effects on chemical shifts of α-glycine were obtained on the basis of probability histograms of selected geometry parameters. Probability distributions of N–H, C–H, C–O, C–C, and C–N bond distances and C–N–H, C–C–N, C–C–O, C–C–H, and H–C–H valence angles, i.e. all bond distances and a set of independent valence angles in glycine molecule, were extracted from the MD and PIMD simulations. This approach based on 1D cross-sections through the shielding surface is much less computationally expensive than a full multidimensional parameterisation. As the 1D method is appropriate only if individual coordinates contribute to the nuclear shielding independently, we checked the additivity by calculating the shielding dependences on one N–H distance for three different C–N–H angles. The calculated dependencies obtained by the 1D and 2D approaches were within 0.01 ppm (see details in the SI). The PIMD distance/angle probabilities were determined independently for all 16 replicas and then averaged. The isotropic shielding was calculated for a coordinate range comprising at least 90% of the structures found in the trajectories, (e.g. 0.85–1.45 Å for the N–H distances, and 100–130° for the C–N–H angles), with 0.1 Å step for the distances and 10° step for the angles, leading to a total of 83 NMR calculations. The dependence of the shielding on the geometrical parameters was approximated by a quadratic function. The probability distributions and the quadratic functions (shown in the SI) were then used to calculate weighted averages of shielding values of glycine for each investigated temperature. The quadratic functions approximated the studied shielding surface very well, with correlation coefficients, R^2, always

higher than 0.99 (see Figure S4 in the SI). The degree of the fitting polynomial can, obviously, be increased if required, at negligible computational cost.

A similar procedure for the calculation of temperature effects was applied to nitromalonamide, where the dependencies of all six independent components of the symmetric electric field gradient tensor on the O–D distance and C–O–D angle were approximated by cubic functions. The O–D and C–O–D probability distributions obtained from MD/PIMD simulations were then convoluted with the cubic functions to obtain average EFG tensor components for given temperature. Diagonalisation of the EFG tensor provided the quadrupolar couplings.[58]

Temperature effects can also be estimated by averaging NMR parameters for individual PIMD snapshots. However, the computation cost is high as NMR calculations would be required for all 16 replicas at every snapshot. We have compared the functional and snapshot approaches in our previous work[37] on the effects of isotopic substitution, observing that the statistical error of the snapshot approach was about one order of magnitude larger than the isotopic shifts being calculated. The temperature effects studied here are even smaller, and so an excessively high number of snapshots would be required for reasonable predictions.

For comparison to the full simulations, a one-dimensional N–H potential was calculated as the DFT energy of the periodic GLYCIN20 structure as a function of the N–H1 distance from 0.8 ... 1.6 Å in 0.025 Å increments. Then the Schrödinger equation was solved numerically, using the reduced mass ($m_N m_H/(m_N + m_H)$) and a plane wave basis set of 40 sine and cosine functions. One-dimensional probability was calculated as $p(x) = \sum_i \exp(-E_i / kT)\varphi_i(x)^2 / \sum_i \exp(-E_i / kT)$, where Ei and φi are energy and wavefunction of a state i, and x is the N–H distance. The probability then could be compared with the MD and PIMD histograms.

Results

Temperature effect on isotropic shieldings in solid α-glycine

Excitation of vibrations will result in both local dynamics and overall changes in unit cell dimensions.[59] It is possible, in principle, to treat these in a uniform way by allowing the unit cell to vary in the MD simulation. For molecular systems, including dispersion corrections would then be essential. However, test computations with empirical dispersion correction[60] indicated that a large energy cutoff of at least 600 eV is needed to reproduce experimental lattice parameters (Table S6 in the SI) well, because the convergence of the stress tensor with respect to the cutoff energy was slower than for the energies and atomic forces. Hence for computational efficiency, we consider the temperature effects on the overall cell dimensions separately from local dynamics. Therefore, for the calculations presented in Table 1, we take into account the effect of cell expansion on shielding by static calculations of shielding values starting from neutron diffraction structures of α-glycine acquired at different temperatures.[38] The atomic positions were optimised to avoid apparent shortening of bond distances with increasing temperature caused by vibrational/librational motions.[21]

The higher-frequency vibrational motions lead to changes of probability distributions of molecular coordinates, which can be obtained from the molecular dynamics trajectories. For example, Figure 2 shows MD and PIMD probability distributions of the C–N and N–H bond distances in α-glycine. As expected, the atoms, especially hydrogens, are more delocalised in the PIMD simulations than in MD. Averaged PIMD values are also shifted slightly towards longer bond lengths.

Increasing the temperature leads to an unrealistic broadening of the classical nucleus MD probability distributions and consequent overestimation of the temperature dependence of NMR

shieldings (Table 1). The quantum PIMD distributions, on the other hand, are almost temperature independent; only slight changes towards longer bonds and broader distributions can be seen at higher temperatures (Figure 2).

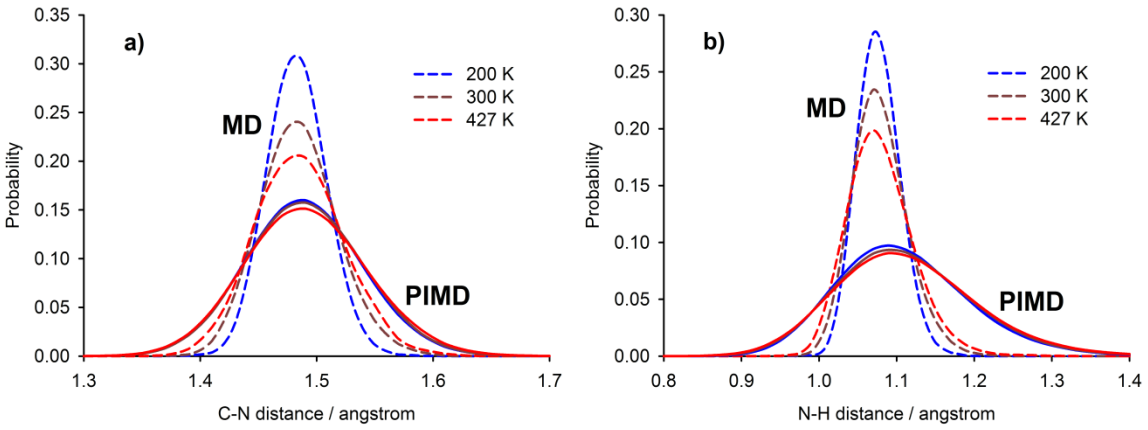

Figure 2. a) C–N and b) N–H distance probabilities found in MD/PIMD simulations of α-glycine at three temperatures.

For comparison, classical and quantum (based on the Schrödinger equation) distance probabilities were calculated for the one-dimensional N–H bond potential (Figure 3). This approach of 1D scans through potential energy landscapes is commonly used for vibrational averaging of molecular properties. The conventional MD probability is closer to the 1D classical distribution, and PIMD distribution is closer to the 1D quantum result. A more detailed look reveals, however, that in both cases the 1D approximation provides narrower distributions than the corresponding MD simulations. This can be attributed to the neglecting of coupling of vibrational dynamics between individual coordinates in the 1D model. Note that the one-dimensional N–H potential was obtained at zero temperature by changing the H atom position only, with all other atoms fixed. In the (PI)MD simulations all atoms could move, and the NH stretching is coupled with other vibrational modes of glycine. Moreover, changes of short

intermolecular distances with neighbouring molecules may lead to ‘squeezing’ or ‘stretching’ of the bond distance during the (PI)MD simulations leading to a non-zero probability in a broader range than that obtained from the one-dimensional potential. The contribution of the contacts, however, appears minor as estimated separately by performing a simulation on a supercell of GLYCIN20 structure with fixed positions of one half of oxygen and nitrogen atoms interconnected by hydrogen bonds (Figure S5 in the SI). This suggests that while 1D potential energy scans may help understand the dynamics phenomena, they are not appropriate for accurate vibrational averaging of spectroscopic properties.

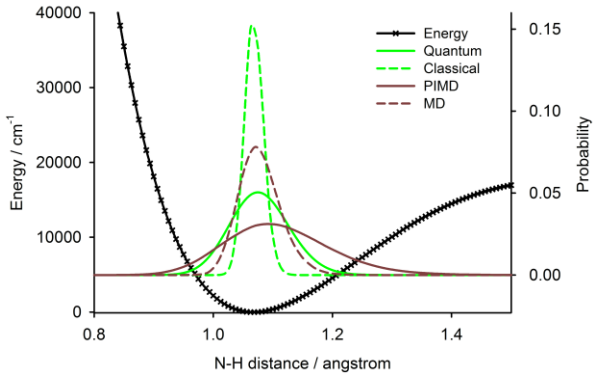

Figure 3. The one-dimensional N–H bond potential, and classical (green, dashed) and quantum (green, solid) probabilities at 300 K calculated from it. The probabilities are compared to the PIMD (brown, solid) and MD (brown, dashed) ones obtained from the full-dimensional simulations.

Contributions of individual coordinates to the temperature effects on NMR shieldings were obtained by convoluting the dependence of the shielding on each coordinate with the MD/PIMD probability histogram of the coordinate for each investigated temperature. In other words, the temperature information is supplied to the NMR averaging via the coordinate dispersion. We

use this "functional" approach, instead of direct NMR calculations for geometry snapshots from the simulation trajectories, because it significantly reduces the computational time and avoids the slow convergence of calculated NMR data with the number of snapshots; we used 83 NMR calculations whereas several hundreds or thousands NMR calculations for geometry snapshots for each temperature would be necessary to achieve good convergence necessary for the prediction of the temperature effects (see Figure S6 showing the convergence of calculated chemical shifts with the number of snapshots), furthermore, 16 NMR calculations would be necessary for every snapshot from the PIMD simulations using 16 beads. A similar approach when the geometry dispersion was used as a secondary variable was successfully used to reduce number of the clusters also for calculation of other molecular properties.[61]

The contributions of all studied coordinates to the temperature changes of NMR shieldings are summarised in Tables S2 and S3 in the SI. As expected, the most important geometry parameters for the temperature effects are those closest to a given nucleus, e.g. the N–H and C–N distances and C–C–N angle for the nitrogen atom, etc., and most of the temperature effect is captured when only bond distances and valence angles involving the studied atom are used for the calculation (SI).

The resultant (PI)MD-determined temperature effects are listed in Table 1. One can see that the magnitudes of the temperature effect on NMR shielding caused by the expansion of the unit cell and by the changes of probability distributions are comparable; however, their signs are sometimes opposite. Only the sum of the PIMD-derived corrections with the static calculations provides excellent agreement with experiment. As discussed above, MD predictions overestimate the effects.

Table 1. Experimental and calculated chemical shift differences (in ppm) of solid α-glycine at 300 and 427 K ($\Delta\delta = \delta_{427\,K} - \delta_{300\,K}$).

Atom	Static[a]	MD-corr.[b]	PIMD-corr.[b]	Static + MD	Static + PIMD	Exp[c]
^{15}N	0.05	0.96	0.48	1.01	0.53	0.61
^{13}C (CO)	–0.17	0.34	0.11	0.17	–0.06	~ –0.20
^{13}C (CH_2)	–0.12	0.63	0.34	0.51	0.22	0.22
^{1}H (NH_3)	0.03	0.00	0.02	0.03	0.05	<0.1
^{1}H (CH_2)	–0.08	0.07	0.03	–0.01	-0.05	<0.1
^{1}H (CH_2)	0.00	0.10	0.06	0.10	0.06	<0.1

[a] Δδ for static calculations on geometry-optimised neutron diffraction structures acquired at 427 and 300 K. [b]Corrections obtained by convoluting shielding surfaces with probablity distributions. [c]Data from ref.,[39] proton chemical shift changes were below spectral resolution of the experiment

Effects on deuterium quadrupolar coupling in NMA

Theoretical predictions of the temperature dependence of quadrupolar couplings are slightly more complicated than those for isotropic chemical shifts, because not only the magnitude but also the orientation of the electric field gradient tensor can be influenced by temperature. Therefore, we calculated the dependence of all six unique components of the EFG tensor on the O–D distance and C–O–D angle and convoluted this dependence with probability distributions of the geometrical parameters obtained from (PI)MD simulations (Figure 4). The magnitude of the quadrupolar coupling was obtained from the principal values of the averaged tensor calculated for a given temperature (Table 2). As before, the classical-nucleus DFT molecular dynamics does not explain the anomalous experimental temperature dependence, but the PIMD approach leads to very good agreement with experiment.

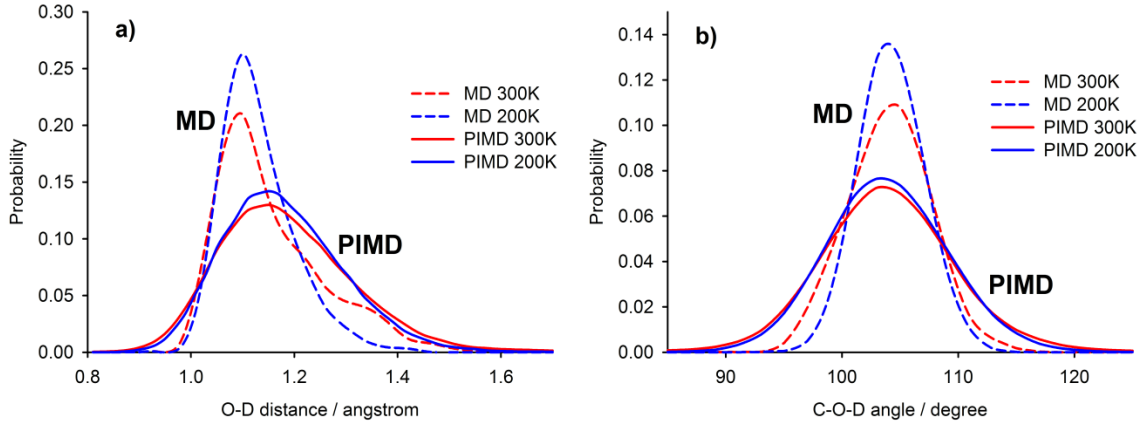

Figure 4. a) O–D distance and b) C–O–D angle probabilities found in MD/PIMD simulations of nitromalonamide at 200 and 300 K.

Table 2. Experimental and calculated difference of deuterium quadrupolar coupling (in kHz) in nitromalonamide at 300 and 200 K, $\Delta C_Q = C_Q(300\ \mathrm{K}) - C_Q(200\ \mathrm{K})$.

	MD	PIMD	Experiment
O–D	–1.4	5.4	
C–O–D	2.4	0.7	
Total	1.0	6.1	6.9

Conclusions

We have demonstrated that the temperature dependence of NMR isotropic shieldings and quadrupolar couplings can be very well rationalized by combining the PIMD simulations with DFT calculations of the shielding and EFG tensors. The functional approach based on convoluting probability distributions with the property surfaces significantly reduced the computational time as it avoided NMR calculations on the geometry snapshots obtained from the dynamics simulations. The combined PIMD/DFT approach reveals detailed relation between the

structure and interactions and NMR parameters, and provides a deep insight into the factors contributing to the temperature effect. The functional approach may also be used for systems where predictions of NMR parameters for a particular atom or region are desired, such as in the case of deuterium quadrupolar coupling in NMA, further saving computational time.

Probability distributions obtained from the PIMD simulations were significantly broader than for the classical-nucleus MD. The difference was most apparent for the light hydrogen nuclei. Conventional MD also led to unrealistic broadening of the probability distributions with increasing temperature. In PIMD simulations, on the other hand, the nuclear delocalisation was about inversely proportional to the temperature, leading to a partial compensation of larger amplitudes of nuclear motion at elevated temperatures. NMR parameters obtained from PIMD probability distributions are, therefore, less temperature dependent than those calculated from classical-nucleus MD trajectories. The comparison with available experimental data clearly indicated that the PIMD approach provides a very good prediction of the temperature effect on NMR shieldings, while conventional-nucleus MD overestimates it. Vibrational averaging based on the 1D scan from potential energy surface, which has recently been used in several studies for prediction of temperature effects, provided a narrower probability distribution for the NH distance than PIMD, because it did not account for vibrational mode coupling and intermolecular interactions in the crystal.

At present, the PIMD approach thus appears as the most universal way to account for the motional averaging in crystals. It accounts both for the molecular dynamics and nuclear quantum effects and may be used for high-quality predictions of spectroscopic parameters at finite temperatures. Although the PIMD approach was applied to molecular crystals, its application to isolated molecules is straightforward. It has already been successfully used for calculations of

deuterium isotope effects on isotropic shifts and scalar couplings in isolated halomethane.[37] Similar application to liquids is possible in principle, although significantly longer simulation times and system sizes are likely to be required in order to reach an ergodic limit.

ASSOCIATED CONTENT

Supporting Information. Additional details of computational methods, additional figures, calculated contributions of individual geometry coordinates to temperature effects, experimental and calculated lattice parameters of α-glycine. This material is available free of charge via the Internet at http://pubs.acs.org.

AUTHOR INFORMATION

Corresponding Author

*Email: dracinsky@uochb.cas.cz

ACKNOWLEDGMENT

The work has been supported by the Czech Science Foundation (grants no. 15-11223S and 15-09072S). The research leading to these results has received funding from the People Programme (Marie Curie Actions) of the European Union's Seventh Framework Programme (FP7/2007-2013) under REA grant agreement n° 299242.

REFERENCES

1. Bonhomme, C.; Gervais, C.; Babonneau, F.; Coelho, C.; Pourpoint, F.; Azais, T.; Ashbrook, S. E.; Griffin, J. M.; Yates, J. R.; Mauri, F.; Pickard, C. J. *Chem. Rev.* **2012,** *112*, 5733-5779.

2. De Dios, A. C.; Jameson, C. J. *Ann. Rep. NMR Spectr.* **2012,** *77*, 1-80.

3. Tang, S.; Case, D. A. *J. Biomol. NMR* **2007,** *38*, 255-266.

4. Dračínský, M.; Bouř, P. *J. Chem. Theory Comput.* **2010,** *6*, 288-299.

5. Dračínský, M.; Kaminský, J.; Bouř, P. *J. Phys. Chem. B* **2009,** *113*, 14698-14707.

6. Bagno, A.; D'Amico, F.; Saielli, G. *ChemPhysChem* **2007,** *8*, 873-881.

7. Waller, M. P.; Geethalakshmi, K. R.; Bühl, M. *J. Phys. Chem. B* **2008,** *112*, 5813-5823.

8. Rohrig, U. F.; Sebastiani, D. *J. Phys. Chem. B* **2008,** *112*, 1267-1274.

9. Straka, M.; Lantto, P.; Vaara, J. *J. Phys. Chem. A* **2008,** *112*, 2658-2668.

10. Kongsted, J.; Nielsen, C. B.; Mikkelsen, K. V.; Christiansen, O.; Ruud, K. *J. Chem. Phys.* **2007,** *126*, 034510.

11. Mort, B. C.; Autschbach, J. *J. Am. Chem. Soc.* **2006,** *128*, 10060-10072.

12. Dračínský, M.; Hodgkinson, P. *RSC Advances* **2015,** *5*, 12300-12310.

13. Dračínský, M.; Kaminský, J.; Bouř, P. *J. Chem. Phys.* **2009,** *130*, 094106.

14. Pickard, C. J.; Mauri, F. *Phys. Rev. B* **2001,** *6324*, 245101.

15. Harris, R. K.; Hodgkinson, P.; Pickard, C. J.; Yates, J. R.; Zorin, V. *Magn. Reson. Chem.* **2007,** *45*, S174-S186.

16. Zheng, A.; Liu, S. B.; Deng, F. *J. Comput. Chem.* **2009,** *30*, 222-235.

17. Holmes, S. T.; Iuliucci, R. J.; Mueller, K. T.; Dybowski, C. *J. Chem. Phys.* **2014,** *141*.

18. Holmes, S. T.; Iuliucci, R. J.; Mueller, K. T.; Dybowski, C. *J. Chem. Theory Comput.* **2015,** *11*, 5229-5241.

19. Dračínský, M.; Jansa, P.; Ahonen, K.; Buděšínský, M. *Eur. J. Org. Chem.* **2011**, 1544-1551.

20. Dumez, J. N.; Pickard, C. J. *J. Chem. Phys.* **2009,** *130*, 104701.

21. Dračínský, M.; Hodgkinson, P. *CrystEngComm* **2013,** *15*, 8705-8712.

22. De Gortari, I.; Portella, G.; Salvatella, X.; Bajaj, V. S.; van der Wel, P. C. A.; Yates, J. R.; Segall, M. D.; Pickard, C. J.; Payne, M. C.; Vendruscolo, M. *J. Am. Chem. Soc.* **2010,** *132*, 5993-6000.

23. Robinson, M.; Haynes, P. D. *J. Chem. Phys.* **2010,** *133*, 084109.

24. Schmidt, J.; Sebastiani, D. *J. Chem. Phys.* **2005,** *123*, 074501.

25. Dračínský, M.; Šála, M.; Hodgkinson, P. *CrystEngComm* **2014,** *16*, 6756-6764.

26. McQuarrie, D. A., *Statistical Thermodynamics*. Harper & Row Publishers: New York, 1973.

27. Hudecová, J.; Hopmann, K. H.; Bouř, P. *J. Phys. Chem. B* **2012,** *116*, 336-342.

28. Rossano, S.; Mauri, F.; Pickard, C. J.; Farnan, I. *J. Phys. Chem. B* **2005,** *109*, 7245-7250.

29. Monserrat, B.; Needs, R. J.; Pickard, C. J. *J. Chem. Phys.* **2014,** *141*, 134113.

30. Janoschek, R. *Mol. Phys.* **1996,** *89*, 1301-1311.

31. Ruden, T. A.; Lutnæs, O. B.; Helgaker, T.; Ruud, K. *J. Chem. Phys.* **2003,** *118*, 9572-9581.

32. Mort, B. C.; Autschbach, J. *J. Phys. Chem. A* **2005,** *109*, 8617-8623.

33. Dračínský, M.; Bouř, P. *J. Comput. Chem.* **2012,** *33*, 1080-1089.

34. Ruud, K.; Åstrand, P. O.; Taylor, P. R. *J. Am. Chem. Soc.* **2001,** *123*, 4826-4833.

35. Åstrand, P. O.; Ruud, K. *Phys. Chem. Chem. Phys.* **2003,** *5*, 5015-5020.

36. Feynman, R. P.; Hibbs, A. R., *Quantum Mechanics and Path Integrals*. McGraw-Hill: New York, 1965.

37. Dračínský, M.; Hodgkinson, P. *Chem. Eur. J.* **2014,** *20*, 2201-2207.

38. Langan, P.; Mason, S. A.; Myles, D.; Schoenborn, B. P. *Acta Cryst. B* **2002,** *58*, 728-733.

39. Taylor, R. E.; Dybowski, C. *J. Mol. Struct.* **2008,** *889*, 376-382.

40. Stievano, L.; Tielens, F.; Lopes, I.; Folliet, N.; Gervais, C.; Costa, D.; Lambert, J. F. *Cryst. Growth Des.* **2010,** *10*, 3657-3667.

41. Simonsen, O.; Thorup, N. *Acta Crystallogr. B* **1979,** *35*, 432-435.

42. Madsen, G. K. H.; Wilson, C.; Nymand, T. M.; McIntyre, G. J.; Larsen, F. K. *J. Phys. Chem. A* **1999,** *103*, 8684-8690.

43. Durlak, P.; Mierzwicki, K.; Latajka, Z. *J. Phys. Chem. B* **2013,** *117*, 5430-5440.

44. Zhao, X. G.; Rossi, P.; Barsegov, V.; Zhou, J.; Woodford, J. N.; Harbison, G. S. *J. Mol. Struct.* **2006,** *790*, 152-159.

45. Kalsbeek, N.; Schaumburg, K.; Larsen, S. *J. Mol. Struct.* **1993,** *299*, 155-170.

46. Miyakubo, K.; Nakamura, N. *Z. Naturforsch.* **2002,** *57*, 337-342.

47. Berglund, B.; Vaughan, R. W. *J. Chem. Phys.* **1980,** *73*, 2037-2043.

48. Limbach, H. H.; Pietrzak, M.; Sharif, S.; Tolstoy, P. M.; Shenderovich, I. G.; Smirnov, S. N.; Golubev, N. S.; Denisov, G. S. *Chem. Eur. J.* **2004,** *10*, 5195-5204.

49. Allen, F. H. *Acta Cryst. B* **2002,** *58*, 380-388.

50. Clark, S. J.; Segall, M. D.; Pickard, C. J.; Hasnip, P. J.; Probert, M. J.; Refson, K.; Payne, M. C. *Z. Kristallogr.* **2005,** *220*, 567-570.

51. Vanderbilt, D. *Phys. Rev. B* **1990,** *41*, 7892-7895.

52. Monkhorst, H. J.; Pack, J. D. *Phys. Rev. B* **1976,** *13*, 5188-5192.

53. Perdew, J. P.; Burke, K.; Ernzerhof, M. *Phys. Rev. Lett.* **1996,** *77*, 3865-3868.

54. Moreira, P. A. F. P.; de Koning, M. *Phys. Chem. Chem. Phys.* **2015,** *17*, 24716-24721.

55. Cao, J. S.; Berne, B. J. *J. Chem. Phys.* **1989,** *91*, 6359-6366.

56. Ceperley, D. M. *Rev. Mod. Phys.* **1995,** *67*, 279-355.

57. Tuckerman, M. E.; Marx, D.; Klein, M. L.; Parrinello, M. *J. Chem. Phys.* **1996,** *104*, 5579-5588.

58. Apperley, D. C.; Harris, R. K.; Hodgkinson, P., *Solid-State NMR: Basic Principles & Practice*. Momentum Press: New York, 2012.

59. Willis, B. T. M.; Pryor, A. W., *Thermal Vibrations in Crystallography*. Cambridge University Press: Cambridge, 1975.

60. McNellis, E. R.; Meyer, J.; Reuter, K. *Phys. Rev. B* **2009,** *80*, 205414.

61. Kessler, J.; Dračínský, M.; Bouř, P. *J. Comput. Chem.* **2013,** *34*, 366-371.

For Table of Contents only

Temperature dependence of NMR parameters calculated from path integral molecular dynamics simulations

Martin Dračínský, Petr Bouř, Paul Hodgkinson